IEEE Access
Multidisciplinary | Rapid Review | Open Access Journal

Received February 27, 2018, accepted April 16, 2018, date of publication April 24, 2018, date of current version May 24, 2018.

Digital Object Identifier 10.1109/ACCESS.2018.2829841

An Accurate Filtenna Synthesis Approach Based on Load-Resistance Flattening and Impedance-Transforming Tapped-Feed Techniques

SHIH-CHENG LIN[1], (Member, IEEE), PIN-YAO CHIOU[2], YI-MING CHEN[2], (Member, IEEE), AND SHENG-FUH CHANG[2], (Senior Member, IEEE)

[1]Department of Electrical Engineering, National Chiayi University, Chiayi 60004, Taiwan
[2]Department of Electrical Engineering, Advanced Institute for Manufacturing With High-tech Innovations, National Chung Cheng University, Chiayi 600, Taiwan

Corresponding author: Shih-Cheng Lin (sclin@mail.ncyu.edu.tw)

This work was supported by the Ministry of Science and Technology of Taiwan under Grant MOST 105-2221-E-415-002, Grant MOST 106-2221-E-415-002, Grant MOST 105-2221-E-194-012, Grant MOST 105-2622-E-194-001-CC1, and Grant MOST 105-2923-E-194-004-MY3.

ABSTRACT In this paper, an accurate filtenna synthesis approach is investigated and verified for achieving the expected filtering response. The load-resistance flattening technique is carried out by attaching the shunt inductive/capacitive elements to cancel the unwanted parasitic element in the antenna model. The synthesis procedure was presented for a filtenna using a planar inverted-F antenna based on parallel-coupled lines. Furthermore, to economize the circuit area, hairpin resonators are adopted to replace the straight resonators in the PCL filtenna, and a tapped-feed structure is utilized for feeding. Thorough investigation reveals that conventional tapped-line feeds based on a singly loaded resonator adopted in a generic coupled-resonator filter requires careful modification to retrieve zero-reactance at the operation frequency. For verification, two bandpass filters were designed with hairpin uniform-impedance and stepped-impedance resonators, thereby validating the practicality of the proposed impedance-transforming tapped feeds. Eventually, the load-resistance flattening and impedance-transforming tapped-feed techniques are combined for developing an accurate filtenna synthesis approach. Two filtennas taking advantage of inverted-L and slotline antennas were designed and fabricated, thus, validating the feasibility of the proposed approach.

INDEX TERMS Filtenna, coupled-resonator filter, load-resistance flattening, impedance transforming, tapped feed, planar inverted-F antenna, inverted-L antenna, slotline antenna.

I. INTRODUCTION

IN an radio-frequency (RF) front-end circuit, there are usually bandpass filters adjacent to antennas for blocking the unwanted interferences or suppressing adjacent channels as shown in Fig. 1. The input/output (I/O) filter ports are commonly designed with Z_0 (usually 50 Ω) for convenience. The conventional approach of designing antennas consists of adjusting the dimensions to make them resonate at the operation frequency f_0 as well as tuning their input resistance to match the output resistance of the preceding stage [1], [2]. However, antenna resistance is limited by the nature of the radiation and may not be easily controlled to the demanded level. Therefore, the antenna resonance is unused. One may take advantage of an impedance transformer between the antenna and filter but sacrifice the insertion loss. If one can carry out the integrated design of the antenna and filter (see Fig. 2) according to the approach of a coupled-resonator filter, it is not necessary to separately design the antenna and filter for matching Z_0.

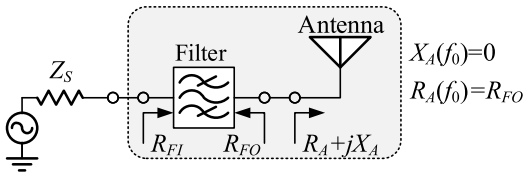

FIGURE 1. Filtenna: co-design of the filter and antenna.

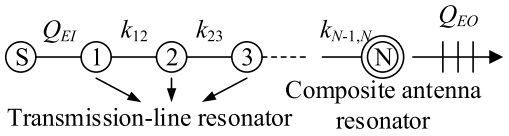

FIGURE 2. Coupling and routing diagram of an *N*th-order filtenna.

A significant amount of research has been conducted to design the so-called filtering antennas (filtennas) with dual function [3]–[8] by elaborately including the antenna resonance in the filter. Extended studies of duplex filtennas [9], dualband filtennas [10], and filtenna arrays [11], [12] have been published. In [3], it was the first time that the filtenna synthesis was proposed by taking advantage of the antenna lumped-element model. However, in the design procedure, three key assumptions, which will be discussed in detail later, are imposed in order to make the synthesis workable. The coupled-resonator filter theory by virtue of full-wave electromagnetic (EM) simulation for extracting the required coupling coefficients and input/output external quality factors is employed in [7], but the authors assumed the output external quality factor of the filtenna Q_{EO} to be approximately equal to the antenna radiation quality factor Q_r to ease the extraction, thus leading to certain inaccuracy. An approach similar to [7] without demanding the antenna model is used in realizing a patch antenna including filtering functionality [8]. The electrically small monopole filtennas are based on capacitively loaded resonators [13]. Nevertheless, to the best of the authors' knowledge, the flatness of the antenna input resistance vs. frequency has not been considered in filtenna design. Intuitively, the dispersion characteristics of the antenna resistance may inevitably affect the filtering performance, and an accurate filtenna design procedure is demanded for achieving the expected filtering response.

Moreover, the feeding structures play an important role in designing the components with filtering characteristics. There are several approaches, such as the tapped-line [14], edge-coupled [15], [16], broadside-coupled [17]–[19], end-coupled [20], [21] feeds and so on, for implementing the feeding function. The tapped-line feeds were adopted in filtennas [8] and [13], and they have been widely exploited for decades in designing a considerable number of coupled-resonator bandpass filters (BPFs) [22]–[25] due to their usage simplicity. The design theory of tapped-line feeds applicable for half-wave (λ/2) open-circuited (OC) uniform-impedance resonators (UIRs) or stepped-impedance resonators (SIRs) is based on a singly loaded resonator [14], [26] and will be proven to not be accurate enough hereafter in this study. Although Y-TF feeds suitable for the bandpass filters using short-circuited resonators were proposed in [27], no corresponding work on accurate tapped feeds for λ/2 OC-SIRs can be found in the literature.

In this study, to more accurately design the filtenna, a compensation technique for flattening the load resistance vs. frequency is adopted in designing a filtering antenna. In addition, accurate tapped feeds with impedance transforming capability applicable in those filters/filtennas utilizing λ/2 OC-SIRs are proposed to tackle the long-standing inaccuracy issue in the field of coupled-resonator filters. Based on load-resistance flattening and the impedance-transforming tapped-feed techniques, an accurate filtenna synthesis approach is developed.

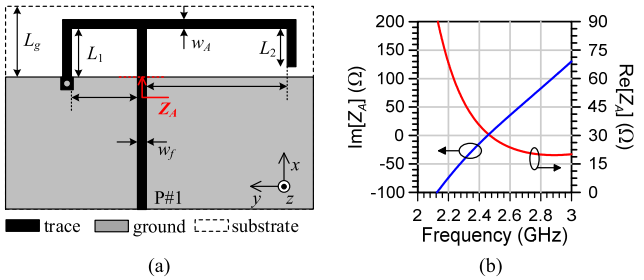

FIGURE 3. Typical PIFA. (a) Layout. (b) EM-simulated input impedance Z_A.

II. REVISITED FILTENNA DESIGN BASED ON LOAD-RESISTANCE FLATTENING

The planar inverted-F antenna (PIFA) is extensively applied in miniaturized wireless devices due to its low profile, quasi-omnidirectional pattern, and ease in matching. Shown in Fig. 3(a) is the layout of a typical PIFA, and Fig. 3(b) illustrates the input impedance Z_A de-embedded to the cutting edge of the ground plane. The equivalent-circuit model consists of a series RLC resonators shunted by an inductor to ground. The resistance R_{ant} is the sum of the ohmic-loss resistance R_{loss} and the radiation resistance R_{rad}. The two specific frequencies are determined by

$$f_A = f|_{Im[Z_A]=0} \quad \text{and} \quad f_{ser} = 1\Big/2\pi\sqrt{L_{ant}C_{ant}}, \tag{1}$$

where $f(=\omega/2\pi)$ is defined as the frequency variable, f_A is the zero-reactance frequency of the overall antenna, and f_{ser} denotes the series resonant frequency of the embedded series RLC. As shown in Fig. 4(a), the PIFA intrinsically possesses rapidly changing input resistance R_A (−65 Ω/GHz) around the zero-reactance frequency of $f_A = 2.45$ GHz and, thus, can hardly be considered as a simple load resistor among the passband. Obviously, the additional inductor complicates the antenna resonant behavior. In designing a filtenna using an antenna as its load, it is straightforward to adjust the frequency f_A equal to the filter center frequency f_0. However, the significantly dispersive input impedance Z_A, especially the real part expressed as

$$R_A = \frac{C_s^2 L_p^2 R_s \omega^4}{1 + C_s(-2(L_p + L_s) + C_s R_s^2)\omega^2 + C_s^2(L_p + L_s)^2\omega^4}, \tag{2}$$

may jeopardize the designated passband. In other words, the better strategy is to control $f_{ser} = f_0$ and try to eliminate the effect of inductor L_p. By attaching a C_p capacitor in parallel with L_p, as shown in Fig. 4(b), the real part R_{AC} of the

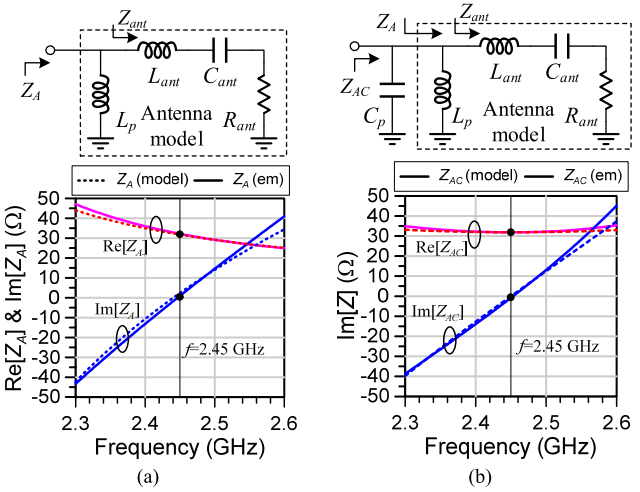

FIGURE 4. Input impedance. (a) Original antenna model ($f_A = f_0 = 2.45$ GHz). (b) Antenna model with flattened load resistance ($f_{ser} = f_0 = 2.45$ GHz).

compensated input impedance Z_{AC} vs. frequency is significantly flattened, thus showing zero slope at f_0. Consequently, the compensated antenna possesses better characteristics for the filtenna purpose.

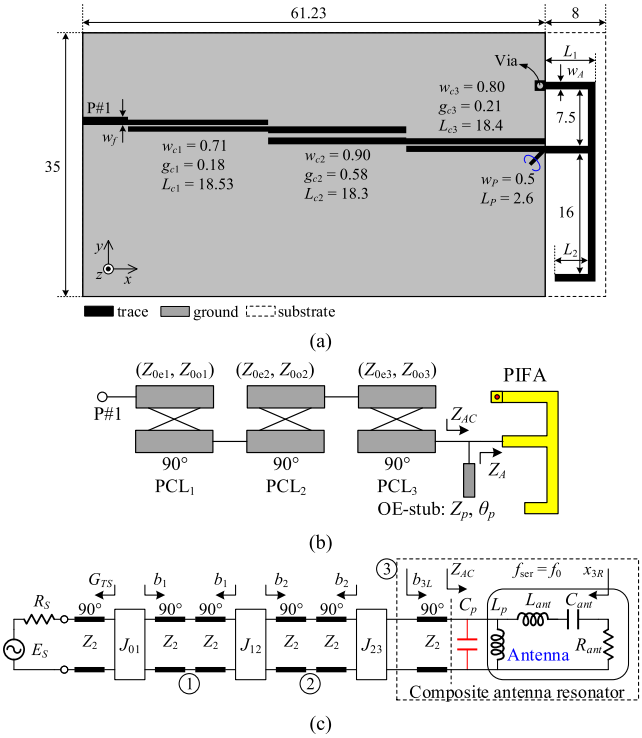

FIGURE 5. Proposed filtenna based on the compensated PIFA with flattened load resistance. (a) Layout. (b) Functional schematic. (c) Inverter-based equivalent circuit of the proposed PIFA filtenna designed at f_0 ($Z_2 = R_S$, $Y_2 = 1/Z_2$, $G_{TS} = R_2/Z_2^2$, Z_2: image impedance of PCL).

Fig. 5(a) depicts the layout of the proposed filtenna using a PIFA with flattened resistance, and its functional schematic and equivalent circuit are shown in Fig. 5(b) and 5(c), respectively. The design concept is based on Cohn's work [15] (see Fig. 6). Note that the image impedances $Z_2(= 1/Y_2)$ of all the open-ended parallel-coupled line (OE-PCL) sections are identical to maintain uniform resonators. Therefore, the filtenna is composed of two OC-UIRs and one composite antenna resonator. The susceptance slope parameters of resonators 1 and 2 are given by

$$b_i = Y_2\pi/2, \quad i = 1, 2. \tag{3}$$

The input admittance seen from the LHS of resonator 3 around the center frequency $f = f_0 + \Delta f$ can be approximated as

$$Y_{3L} = Y_2^2/Y_{AC}, \quad \text{with} \quad Z_{AC} = 1/Y_{AC} = j2L_{ant}(2\pi\Delta f). \tag{4}$$

The susceptance slope parameter b_{3L} can be calculated by

$$b_{3L} = \frac{f_0}{2}\frac{\partial Im[Y_{3L}]}{\partial f}\bigg|_{f=f_{res}} = Y_2^2(2\pi f_0 L_{ant}). \tag{5}$$

Furthermore, according to Fig. 5, the input impedance Z_{3R} seen from the RHS of resonator 3 consists of a series LC resonator cascaded by an open-ended $\lambda/4$ resonator. The reactance slope parameter x_{3R} seen from the RHS of resonator 3 can be calculated by the sum of the two individual resonators

$$x_{3R} = 2\pi f_0 L_{ant} + \pi Z_2/4, \tag{6}$$

thus forming the so-called composite antenna resonator. It is interesting to note that resonator 3 behaves as a series resonator when observed from the RHS but alternatively as a parallel resonator when observed from the LHS.

Eventually, based on [28], the inverter values are expressed as

$$J_{01} = \sqrt{\frac{G_{TS}\Delta \cdot b_1}{g_0 g_1}}, \quad J_{12} = \sqrt{\frac{\Delta^2 b_1 b_2}{g_1 g_2}}, \text{ and}$$
$$J_{23} = \sqrt{\frac{\Delta^2 b_2 b_{3L}}{g_2 g_3}}, \tag{7}$$

where g_i denotes the element values of the lowpass prototype and Δ is the fractional bandwidth. For design convenience, Z_2 can be selected equal to R_S making $G_{TS} = G_S$. With regard to the loaded antenna, the corresponding external quality factor Q_{EO} related to series resonance with respect to R_{ant} is

$$Q_{EO} = x_{3R}/R_{ant} = Q_{ant} + \pi Z_2/(4R_{ant}) \tag{8}$$

where $Q_{ant}(= \omega_0 L_{ant}/R_{ant})$ is the radiation quality factor of the compensated antenna. Note that Q_{ant} and R_{ant} are both relevant to antenna size and thus have to be extracted with the aid of the full-wave EM simulator. In this study, the full-wave simulations and optimizations were performed using the ANSYS HFSS while the circuit-level simulations are carried out by NI AWR Design Environment. Fig. 7 exhibits the design graph of the extracted external quality factor Q_{EO}

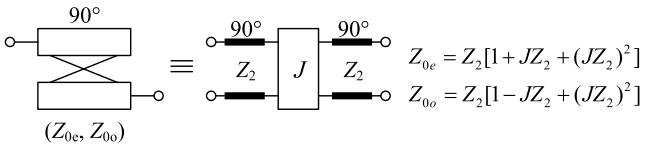

FIGURE 6. Equivalent circuit of the PCL section (Cohn's approach).

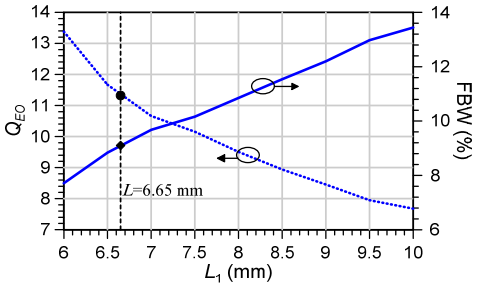

FIGURE 7. Design graph of the extracted output external quality factor Q_{EO} and corresponding fractional bandwidth FBW versus length L_1 based on (8).

and the fractional bandwidth versus length L_1. The realizable bandwidth ranges from 7.7% to 13.4% as L_1 ranges from 6 to 10 mm. Relatively, the patch antenna lacks of flexibility in dimension selection thus the designable bandwidth in filtenna application may be restricted.

For demonstration, two filtennas, i.e., PIFA1 and PIFA2, are realized based on two different approaches $f_{ser} = f_0$ with flattening and $f_A = f_0$ without flattening, respectively, to reveal the necessity of flattened load resistance. Both filtennas are designed for a 3rd-order Chebyshev response with ripple = 0.1 dB, Δ = 9.1%, and source impedance $R_S = 50\ \Omega$. The corresponding element values of the lowpass prototype are $[g_0, g_1, g_2, g_3,$ and $g_4] = [1.0, 1.0316, 1.1474, 1.0316,$ and $1.0]$. The output external quality factor Q_{EO} relevant to the physical dimension L_1 is extracted and calculated according to Fig. 7. The antenna model parameters adopted in the two approaches are summarized in Table 1.

TABLE 1. Filtenna design parameters: PIFA model.

	Frequency (GHz)	Resonator elements
PIFA filtenna 1 (PIFA1) $f_{ser} = f_0$	$f_{ser} = 2.450$ $f_A = 2.435$	$L_p = 18$ nH, $C_p = 0.234$ pF, $L_{ant} = 20.3$ nH, $C_{ant} = 0.2079$ pF, $R_A = 31.9\ \Omega$
PIFA filtenna 2 (PIFA2) $f_A = f_0$	$f_{ser} = 2.466$ $f_A = 2.450$	$L_p = 15$ nH, $C_p = 0$, $L_{ant} = 19.1$ nH, $C_{ant} = 0.2179$ pF, $R_A = 30.5\ \Omega$

Regarding the PIFA1 filtenna, the PIFA structure is adjusted giving $f_{ser} = f_0 = 2.45$ GHz (L_p = 18 nH, L_{ant} = 20.3 nH, C_{ant} = 0.2079 pF, R_{ant} = 31.9 Ω) compensated by an additional capacitor C_p = 0.234 pF implemented by an open-ended stub (Z_{os} = 77 Ω, θ_{os} = 15.5°). The PCL image impedance is selected as Z_2 = 50 Ω. It leads to $b_1 = b_2$ = 31.42 mS, b_{3L} = 132.84 mS, and x_{3R} = 351.76 Ω. The design parameters for the inverter-based

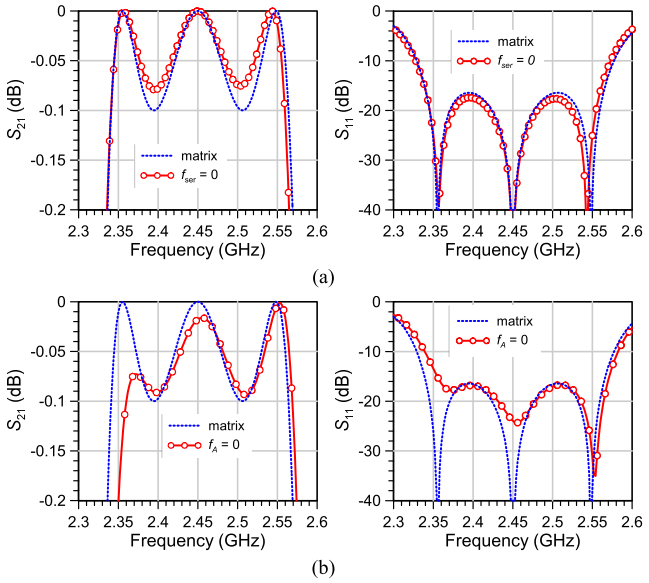

FIGURE 8. Circuit-level simulated two-port scattering parameters using the equivalent circuit of the PIFA filtenna proposed in Fig. 6 treating R_S and R_{ant} as input and output ports, respectively. (a) PIFA1: set $f_{ser} = f_0$ (with flattening). (b) PIFA2: set $f_A = f_0$ (without flattening).

filtenna are J_{01} = 7.55 mS, J_{12} = 2.7 mS, J_{23} = 5.55 mS and Q_{EO} = 11.03. Eventually, the even- and odd-mode impedances for the three PCL sections are (Z_{0e1}, Z_{0o1}) = (75.99, 38.25) Ω, (Z_{0e1}, Z_{0o1}) = (57.67, 44.16) Ω, and (Z_{0e3}, Z_{0o3}) = (67.74, 39.97) Ω. Fig. 8(a) compares the scattering parameters transformed from the ideal coupling matrix to the results simulated based on the circuit in Fig. 5. Satisfactory agreement between the two results in terms of passband ripple and return loss (RL) can be observed showing the validity of the proposed approach.

To clearly reveal the influence of flattening the load resistance, a PIFA2 filtenna is designed using a PIFA without flattening ($f_A = f_0$ = 2.45 GHz) in contrast to the PIFA1 filtenna. Fig. 8(b) compares the scattering parameters transformed from the ideal coupling matrix to the circuit-level simulated results. The passband degrades significantly on the lower band edge due to the increasing resistance slope thus causing bandwidth shrinkage and an asymmetric response. The influence of the resistance unflatness will inevitably become more serious for filtennas with wider bandwidth.

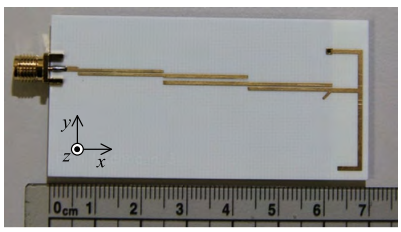

FIGURE 9. Circuit photograph of the proposed PIFA1 filtenna.

The PIFA1 filtenna is then implemented on a RO4003C substrate (ε_r = 3.55, h = 0.813 mm, tanδ = 0.0027) with its circuit photograph exhibited in Fig. 9. The

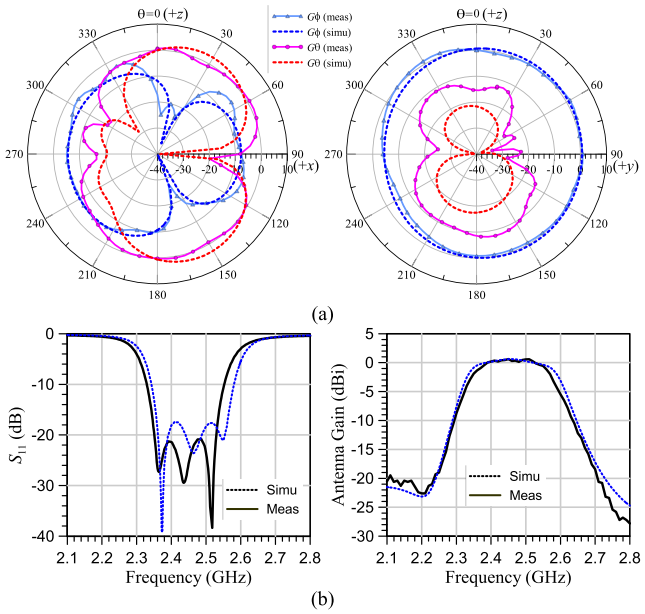

FIGURE 10. EM-simulated/measured results of the PIFA1 filtenna. (a) *xz*- and *yz*-plane radiation patterns. (b) Reflection coefficients and antenna realized gain in the $+z$ direction ($\varphi = 0°$, $\theta = 0°$).

measured and simulated radiation patterns on the *xz*- and *yz*-planes are illustrated in Fig. 10(a). The fabricated filtenna possesses the patterns of gain G_φ in the *yz*-plane and the total gain in the *xz*-plane both nearly omni-directional. The EM-simulated/measured reflection coefficients and the realized antenna gains are shown in Fig. 10(b). The minimum RL among the passband is 21.3 dB, whereas the 15-dB RL bandwidth from 2.342 to 2.538 GHz is related to a ripple-FBW of 8.1%. The bandwidth shrinkage may be attributed to the etching resolution (line width/spacing) of the adopted PCB process. The simulated and measured antenna gains in the $+z$ direction are approximately 0.608 and 0.604 dBi, respectively. The gain drops below -20 dBi at frequencies below 2.24 GHz or above 2.71 GHz because of the integrated filter. The measured results are well predicted by the EM simulation in terms of the passband RL ripple and antenna gain.

Notably, in Chuang's work [3], important contributions were presented, but three assumptions were made to make their synthesis possible: 1) the antenna quality factor is roughly used to estimate the FBW, 2) the symmetric two-port PCL section adjacent to the antenna is modeled as an asymmetric network composed of two TL sections with different characteristic impedance Z_0 and Z_a, and 3) the parasitic capacitor C_g in Fig. 4 of [2] is considered ignorable after circuit transformation. For the 1st assumption, through (8), the output Q_{EO} depends not only on the antenna but also on the $\lambda/4$ TL resonator. With regard to the 2nd assumption, it has been proven that using an asymmetric network to model a symmetric structure is physically not appropriate [29]. For the 3rd assumption, the C_g can roughly be ignored at the center frequency and otherwise found not negligible due to its influence on the antenna frequency response. On the other hand, a thorough synthesis procedure has been proposed in this section without necessitating the three assumptions. Most important of all, the simple analytical design formulas are derived and can be easily extended to Nth-order filtenna design.

III. HAIRPIN FILTER BASED ON ACCURATE IMPEDANCE-TRANSFORMING TAPPED FEEDS

The horizontal dimension of the filtenna utilizing PCL sections can be further miniaturized by using hairpin resonators [30]. Shown in Fig. 11(a) is the sample layout of a conventional 3rd-order hairpin coupled-resonator BPF. The interstage couplings are achieved by open-ended PCLs, whereas the I/O feeds are realized by tapped lines. Taking advantage of the tapped-line feeds, one may more flexibly select the resonator impedance without being restricted by the end PCL section adjacent to the input port. The schematic circuit is given in Fig. 11(b) and deserves careful investigation.

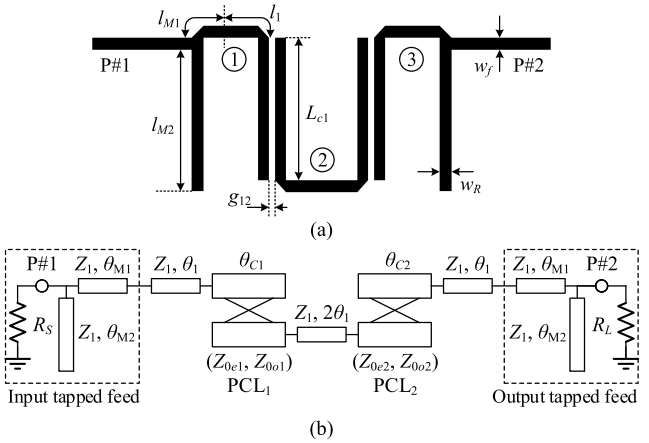

FIGURE 11. Hairpin coupled-resonator filter with impedance-transforming tapped feeds and PCL interstage couplings. (a) Layout. (b) Functional schematic.

A. PARALLEL COUPLED-LINE SECTION

The coupling structure between resonators consists of the OE-PCL sections. Among the PCL filters, each i-th PCL section PCL$_i$ in Fig. 12 of even-/odd-mode characteristic impedances, Z_{0e} and Z_{0o}, used for interstage coupling can be modeled by an impedance inverter attached to two series open-circuited stubs [28]. By providing the coupled length θ_{Ci}, the preferable reference impedance Z_{si}, and the inverter value K_i from the filter parameters, the Z_{0e} and Z_{0o} of i-th PCL section are available as

$$Z_{0ei} = Z_{si} + K_i \sin\theta_{Ci} \tag{9a}$$

$$Z_{0oi} = Z_{si} - K_i \sin\theta_{Ci} \tag{9b}$$

The i-th inverter is determined by both the length θ_{ci} and the impedance $Z_{di}[= (Z_{0ei} - Z_{0oi})/2]$ as

$$K_i = Z_{di}/\sin\theta_{Ci} \quad \text{with} \quad i = 1, 2, \ldots, N-1 \tag{10}$$

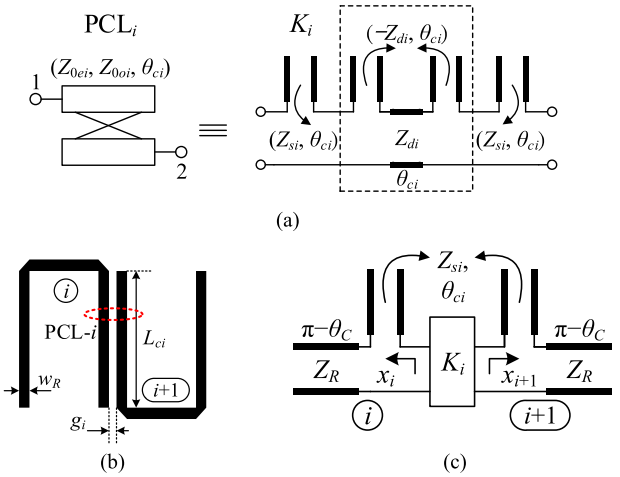

FIGURE 12. Interstage coupling between resonators i and $i+1$ using an OE-PCL. (a) Equivalent circuit of the OE-PCL section. (b) Layout of the coupled-resonator pair. (c) Open-wire equivalent circuit of the coupled-resonator pair ($i = 1, 2$).

Based on (10), an auxiliary graph is drawn in Fig. 13 using Z_{si} and K_i as parameters for demonstration of the impedances (Z_{0ei}, Z_{0oi}) of the i-th PCL section with predetermined coupled length $\theta_{ci} = 70°$. Note that this graph can be easily redrawn under an arbitrarily selected coupled length.

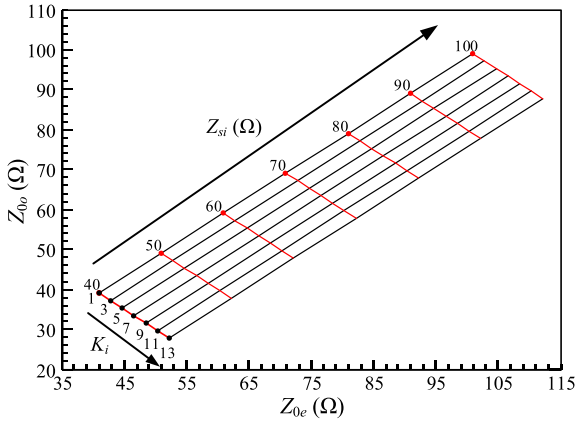

FIGURE 13. Even- and odd-mode characteristic impedances (Z_{0ei}, Z_{0oi}) of i-th PCL section with both reference impedance Z_{si} and inverter value K_i as parameters (coupled length $\theta_{Ci} = 70°$).

B. DISCUSSION OF GENERIC BPFS USING HAIRPIN UIRS WITH CONVENTIONAL TAPPED-LINE FEEDS

For the conventional hairpin coupled-resonator filter using UIRs with the topology as shown in Fig. 11, the electrical lengths must fulfill the following conditions to ensure resonance of each isolated resonator

$$\theta_{M1} + \theta_{M2} + \theta_1 + \theta_{C1} = \pi, \theta_1 + \theta_{C1} = \pi/2, \quad (11a)$$

$$\theta_{C1} + 2\theta_1 + \theta_{C2} = \pi. \quad (11b)$$

Based on the typical design approach of coupled-resonator filters, the I/O feeds and the interstage couplings are independently designed as follows. The tapped position $\theta_{M1} = \theta_E$ can be calculated from the singly loaded resonator ($G_S = 1/R_S$) [14].

$$\theta_E = \beta_g l_{M1} = \sin^{-1}\sqrt{\pi Y_R / 2G_S Q_E}. \quad (12)$$

With regard to the coupling between resonators depicted in Fig. 12, the required impedance inverter values K_1 and K_2 can be expressed as

$$K_1 = K_2 = \sqrt{\frac{\Delta^2 x_1 x_2}{g_1 g_2}} = \frac{\Delta \cdot x_1}{\sqrt{g_1 g_2}}, \quad (13)$$

where the reactance slope parameter of the resonator is

$$x_i = \frac{f_0}{2}\frac{\partial X_i}{\partial f}\bigg|_{f=f_0} = \frac{\pi Z_2}{2}\csc^2\theta_c, \quad i = 1, 2, 3. \quad (14)$$

In accordance with (9)-(14), this conventional hairpin filter can be designed. By applying $Z_R = 50\ \Omega$ as the resonator transmission line (TLIN) impedance, a microstrip 3rd-order filter at $f_0 = 2.45$ GHz is designed for a 0.04321-dB-ripple Chebyshev response with $\Delta = 5\%$. The electrical parameters are $x_i = 88.944\ \Omega$ and $K_{12} = K_{23} = 4.588\ \Omega$. The corresponding Z_{0e} and Z_{0o} of the PCL section can be found through Fig. 13. The calculated electrical parameters are listed in Table 2 as the "Conv." row, whereas the circuit-level simulated results are shown in Fig. 14. Obviously, the passband response of the conventional hairpin filter deviates significantly from ideal one. This is the reason why a coupled-resonator filter demands unexpected dimension tuning even when based exactly on the conventional approach, which means that the conventional design approach requires appropriate modification.

TABLE 2. 3rd-order BPF using hairpin resonators.

	Design parameters	$\theta_{M1}+\theta_{M2}$
Conv.	Z_1=50 Ω, $\theta_{C1}=\theta_{C2}$=70°, θ_1=20°, θ_{M1}=17.68°, θ_{M2}=72.32° $(Z_{0e1}, Z_{0o1}) = (Z_{0e2}, Z_{0o2})$=(54.3115, 45.6885) Ω	90°
This work	Z_1=50 Ω, $\theta_{C1}=\theta_{C2}$=70°, θ_1=20°, θ_{M1}=16.1°, θ_{M2}=72.52° $(Z_{0e1}, Z_{0o1}) = (Z_{0e2}, Z_{0o2})$=(54.1225, 45.8775) Ω	88.62°

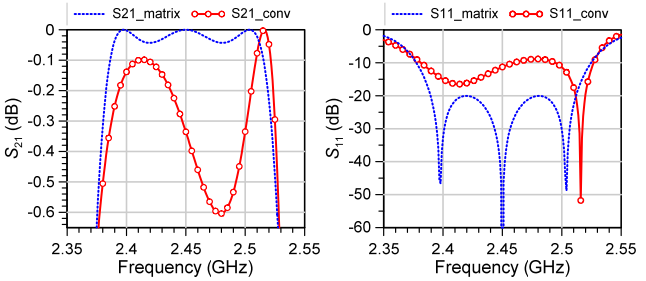

FIGURE 14. Comparison of the S-parameters generated from the circuit simulation using Fig. 11(b) (Conv) and those transformed from the coupling matrix (Matrix).

C. ACCURATE IMPEDANCE-TRANSFORMING TAPPED FEEDS

Fig. 15 exhibits the revised version of the PCL coupled-resonator filter using the hairpin SIRs with the adopted

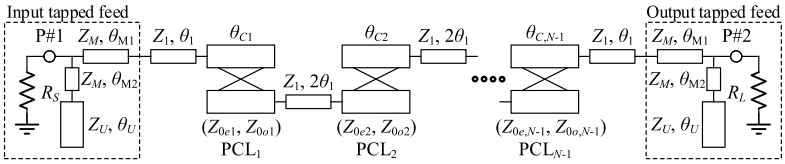

FIGURE 15. Generalized PCL coupled-resonator filter using the hairpin SIRs and the impedance-transforming tapped feeds ($Y_M = 1/Z_M$, $Y_1 = 1/Z_1$, $Y_2 = 1/Z_2$).

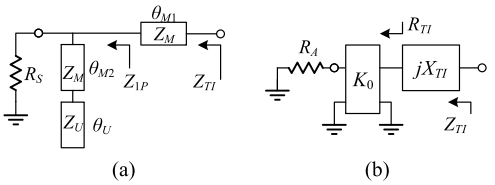

FIGURE 16. Proposed impedance-transforming tapped feed: (a) schematic and (b) equivalent circuit.

impedance-transforming tapped feeds depicted in Fig. 16. The inverter-based open-wire equivalent circuit is shown in Fig. 17. As discussed in Sec. II.A, a different viewpoint on the tapped-feed structure is necessary to acquire a satisfactory filter response. The input impedance of the tapped feed structure for a specified source resistance R_S can be expressed as

$$Z_{TI} = R_{TI} + jX_{TI} = Z_M \frac{Z_{1P} + jZ_M \tan\theta_{M1}}{Z_M + jZ_{1P} \tan\theta_{M1}} \tag{15a}$$

with $Y_{1P} = 1/Z_{1P}$ given as

$$Y_{1P} = 1\Big/R_S + jY_M \frac{Y_U \tan\theta_U + Y_M \tan\theta_{M2}}{Y_M - \tan\theta_U \cdot Y_U \tan\theta_{M2}} \tag{15b}$$

To ensure that the effective resonator 1 resonates at f_0, it is essential to force the input reactances seen from both its sides (LHS and RHS) to simultaneously vanish at f_0, i.e., $X_{1L}(f_0) = X_{1R}(f_0) = 0$. The above condition can be fulfilled by letting $X_{TI}(f_0) = 0$. As a result, the impedance-transforming tapped-feed structure also contributes to the reactance slope for effective resonator 1. The susceptance slope of X_{TI} ($\equiv X'_{1L}$) can be expressed as

$$x_{TI} = \frac{f_0}{2} \frac{\partial X_{TI}}{\partial f}\bigg|_{f=f_0}. \tag{16}$$

According to Fig. 17, the overall reactance observed from the LHS of resonator 1 can be treated as the series combination of the series-LC tank contributed by the series-resonant source and the λ/4 open-circuited SIR. The LHS reactance slope parameter for resonator 1 can be formulated as

$$x_{1L} = x_{TI} + x''_{1L} = x'_{1L} + x''_{1L}, \tag{17}$$

where $x"_{1L}$ represents the LHS susceptance slope parameter of the λ/4 open-circuited SIR shown in Fig. 17 that can be analytically evaluated by

$$x''_{1L} = Z_1 \frac{\sec^2\theta_1 [A_Z\theta_2 \sec^2\theta_2 + \theta_1(A_Z^2 + \tan^2\theta_2)]}{2(A_Z \tan\theta_1 + \tan\theta_2)^2} \tag{18}$$

In addition, the RHS reactance slope parameter x_{1R} for resonator 1 obtained by differentiating the input reactance X_{1R} is

$$x_{1R} = x_{TI} \sec^2\theta_1 + (Z_1\theta_1 \sec^2\theta_1 + Z_2\theta_2 \csc^2\theta_2)\Big/2. \tag{19}$$

Based on the design approach of the inverter-based coupled-resonator bandpass filter, the input coupling has to satisfy the following conditions

$$\frac{K_0^2}{R_A} = R_{TI}(f_0), \quad \text{where} \quad K_0 = \sqrt{\frac{\Delta \cdot R_A \cdot x_{1L}}{g_0 g_1}}. \tag{20}$$

Eventually, the following simultaneous equations for solving θ_{M1} and θ_{M2} at f_0 with the given R_S are summarized as

$$X_{TI}(f_0, R_S, \theta_{M1}, \theta_{M2}) = 0, \tag{21a}$$

$$\frac{x_{1L}(R_S, \theta_{M1}, \theta_{M2})}{R_{TI}(f_0, R_S, \theta_{M1}, \theta_{M2})} \equiv Q_{EI} \text{ with } Q_{EI} \frac{\Delta}{g_0 g_1}. \tag{21b}$$

Similarly, the equations for the arbitrary resonant load port with given R_L are

$$X_{TO}(f_0, R_L, \theta_{M1}, \theta_{M2}) = 0, \frac{x_{NR}(R_L, \theta_{M1}, \theta_{M2})}{R_{TO}(f_0, R_L, \theta_{M1}, \theta_{M2})} \equiv Q_{EO}, \tag{22}$$

where $X_{TO} = \mathrm{Im}[Z_{TO}]$ and $Q_{EO} = \Delta/(g_N \times g_{N+1})$. With regard to the resonator N, the RHS reactance slope parameter $x_{NR} = x'_{NR} + x''_{NR}$ can be similarly derived as x_{1L} in (17), whereas x_{NL} can be similarly derived as x_{1R} in (19).

To clearly reveal the effect of adopting the proposed impedance-transforming tapped feed, consider a loaded resonator designed for external quality factor $Q_E = 17.032$ and $R_S = 50\ \Omega$. The SIR parameters are given as $Z_1 = 90\ \Omega$ and $Z_2 = 45\ \Omega$, and $\theta_1 = \theta_2 = 35.2644°$. By setting $\theta_U = \theta_2$ and $Z_M = Z_1$, the required tapped-line feeding lengths are calculated based on both the modified and conventional approaches, and the simulated Z_{TI} for the two approaches are shown in Fig. 18. Apparently, the non-vanishing imaginary part X_{TI} at f_0 based on the circuit using the conventional approach will detune resonator 1 and thus degrade the filter passband response as observed in Fig. 14.

Based on (9)-(22), the design graphs are drawn in Fig. 19 for finding the lengths of θ_{M1} and θ_{M2}. The proposed impedance-transforming tapped feed has $Q_{EI} = Q_E$ and $R_S = R_0$ as parameters. Fig. 19(a) is calculated for the BPF using hairpin UIRs ($Z_1 = 50\ \Omega$, $Z_2 = 50\ \Omega$, $\theta_{C1} = \theta_{C2} = 70°$, $\theta_2 = 20°$, $\theta_U = \theta_2$, $Z_U = Z_2$, $Z_M = Z_1$), whereas Fig. 19(b) is for the BPF using hairpin SIRs ($Z_1 = 90\ \Omega$,

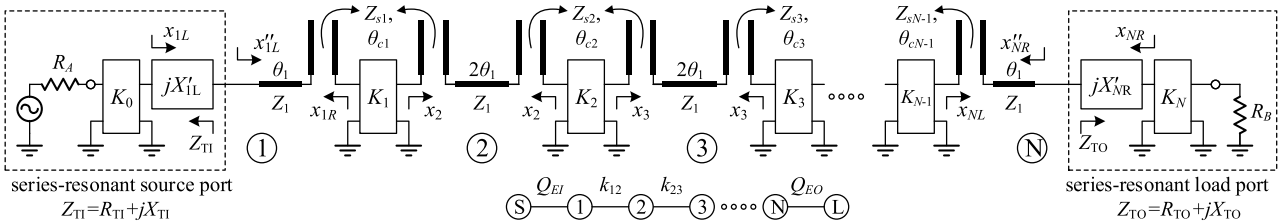

FIGURE 17. Inverter-based open-wire equivalent circuit of the proposed N-th order BPF using hairpin SIRs and impedance-transforming tapped feeds.

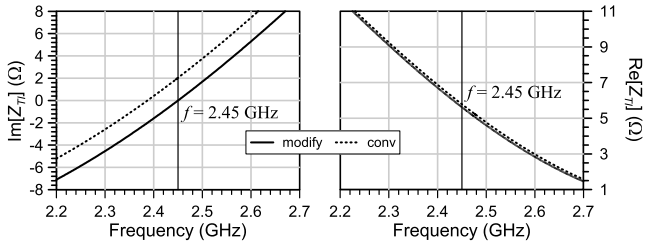

FIGURE 18. Input impedances Z_{TI} seen in the tapped feed. Conventional: $(\theta_{M1}, \theta_{M2}) = (11.56°, 23.7°)$; Modified: $(\theta_{M1}, \theta_{M2}) = (10.1259°, 23.8879°)$.

$Z_2 = 45\ \Omega$, $\theta_1 = \theta_2 = 35.2644°$, $\theta_{c1} = \theta_{c2} = \theta_2$, $\theta_U = \theta_2$, $Z_U = Z_2, Z_M = Z_1$). The required θ_{M1} and θ_{M2} can be readily acquired by locating the assigned (Q_E, R_0) in the figure.

D. DESIGN OF AN INVERTER-BASED COUPLED-RESONATOR FILTER

To design the filter presented in Fig. 15, it is essential to calculate the couplings and external quality factors according to the filter specification (center frequency f_0, fractional bandwidth Δ, filter order N, and lowpass prototype response). Among the filter structure, the impedance-transforming tapped feeds are used to achieve I/O feedings, whereas the open-ended PCL sections are adopted to realize the interstage couplings. The two end resonators with tapped feeds satisfy

$$x_{1L}/R_{TI} = Q_{EI} \quad \text{and} \quad x_{NR}/R_{TO} = Q_{EO}, \tag{23}$$

where x_{1L} denotes the reactance slope parameter of outer resonator 1 seen from the LHS and x_{NR} denotes the reactance slope parameter of outer resonator N seen from the RHS. The electrical lengths θ_{M1} and θ_{M2} of the tapped feeds related to input and output ports can be solved for based on (23). Furthermore, the values of the interstage impedance inverters can be evaluated by

$$K_1 = \sqrt{\frac{\Delta^2 x_{1R} x_2}{g_1 g_2}}, \quad K_{N-1} = \sqrt{\frac{\Delta^2 x_{N-1} x_{NL}}{g_{N-1} g_N}}, \tag{24a}$$

and

$$K_i = \frac{\Delta \cdot \sqrt{x_2 x_3}}{\sqrt{g_i g_{i+1}}} = \frac{\Delta \cdot x_{SIR}}{\sqrt{g_i g_{i+1}}}, i = 2, \cdots, N-2. \tag{24b}$$

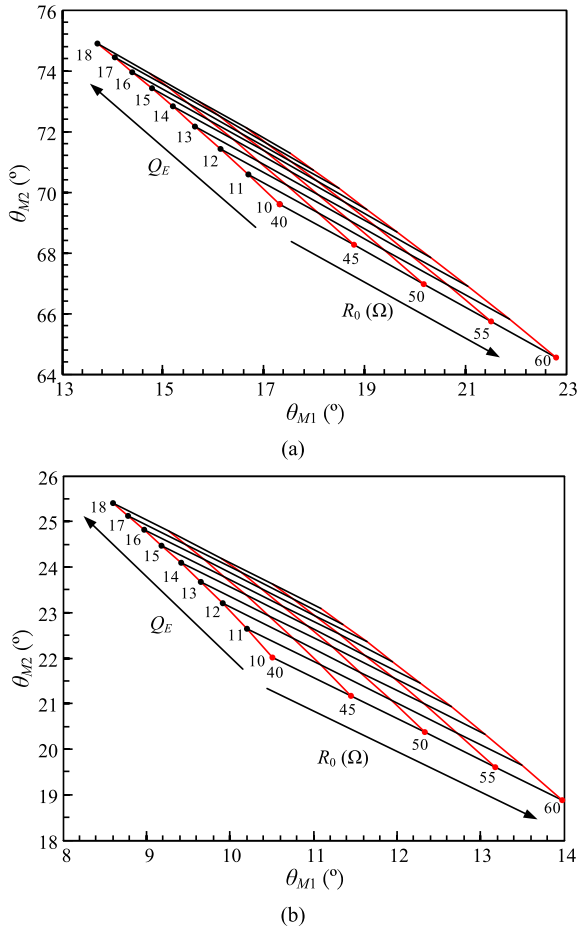

FIGURE 19. Design graphs for finding θ_{M1} and θ_{M2} with Q_E and R_S as parameters. (a) For BPFs using hairpin UIRs. (b) For BPFs using hairpin SIRs.

where $x_i (= x_{SIR})$ denotes the reactance slope parameter of the inner i-th SIRs ($i = 2, \ldots, N-2$) as depicted in Fig. 20. x_{SIR} can be analytically evaluated by

$$x_{SIR} = Z_2\theta_2 \csc^2\theta_2 \Big/ 2 + Z_1 \sec^2 2\theta_1 \times \frac{2(-Z_1^2 + Z_2^2)\theta_1 + Z_1(2Z_1\theta_1 + Z_2\theta_2)\sec^2\theta_2}{2(Z_2 \tan 2\theta_1 + Z_1 \tan\theta_2)^2}. \tag{25}$$

under the resonant condition of the inner resonator

$$\tan\theta_1 \tan\theta_2 = Z_2/Z_1 = A_Z. \tag{26}$$

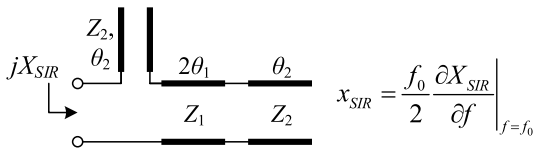

FIGURE 20. Inner TL resonator among the inverter-based filters shown in Fig. 17.

With (23)-(26), the proposed synthesis procedure can be readily adopted in designing a filter with higher order by cascading more PCL sections.

TABLE 3. Parameters of the filters using hairpin resonators.

	BPF1-UIR: 3rd, Δ=5% Chebyshev 0.04321 dB-ripple	BPF2-SIR: 3rd, Δ=5% Chebyshev 0.04321 dB-ripple
Given parameters	Z_1=50 Ω, Z_2 = 50 Ω, A_Z = 1.0, $\theta_{C1}=\theta_{C2}$=70°, θ_1=20°, $\theta_U=\theta_2$, $Z_U=Z_2$, $Z_M=Z_1$	Z_1=90 Ω, Z_2=45 Ω, A_Z = 0.5 $\theta_1=\theta_2$=35.2644°, $\theta_{c1}=\theta_{c2}=\theta_2$, $\theta_U=\theta_2$, $Z_U=Z_2$, $Z_M=Z_1$
Intermediate parameters	$R_{TI}=R_{TO}$=4.17, $x_{1L}=x_{3R}$=70.98, $x_{1R}=x_{3L}$=81.32 Ω, x_{SIR}= 88.94, $K_1=K_2$=4.39 (all unit: Ω)	$R_{TI}=R_{TO}$=5.62, $x_{1L}=x_{3R}$=95.71, $x_{1R}=x_{3L}$=146.57, x_{SIR}=166.18 $K_1=K_2$=8.05 (all unit: Ω)
Final circuit parameters	$(Z_{0e1},Z_{0o1})=(Z_{0e2},Z_{0o2})$= (54.1225, 45.8775) Ω θ_{M1}=16.1°, θ_{M2}=72.52° $\theta_{M1}+\theta_{M2}=88.62° \neq 90°$	$(Z_{0e1},Z_{0o1})=(Z_{0e2},Z_{0o3})$= (49.3685, 40.6315) Ω θ_{M1} = 10.13°, θ_{M2} = 23.89°, $\theta_{M1}+\theta_{M2}=34.02° \neq \theta_1$

E. IMPLEMENTATION OF TWO SAMPLE FILTERS BASED ON THE PROPOSED IMPEDANCE-TRANSFORMING TAPPED-LINE FEEDS

For demonstration, two sample filters, i.e., BPF1-UIR and BPF2-SIR, using hairpin resonators are designed with f_0 = 2.45 GHz, and $\Delta = 5\%$ for a 0.04321 dB-ripple Chebyshev response. The corresponding element values of the lowpass prototype are $[g_0, g_1, g_2, g_3,$ and $g_4] = [1.0, 0.8516, 1.1032, 0.8516,$ and $1.0]$. BPF1-UIR is composed of hairpin UIRs ($Z_1 = Z_2 = 50\ \Omega$, $\theta_1 = 20°$, $\theta_2 = 70°$), and its coupled lengths of PCL sections are $\theta_C = \theta_2$, whereas BPF2-SIR is composed of hairpin SIRs ($Z_1 = 90\ \Omega$, $Z_2 = 45\ \Omega$, $\theta_1 = 35.26°$, $\theta_2 = 35.26°$), and its coupled lengths of PCL sections are $\theta_C = \theta_2$ as well. The final circuit parameters are tabulated in Table 3. From the calculated parameters, it is verified that the proposed impedance-transforming tapped feeds possess different line lengths than the conventional approach.

The circuit-level simulated scattering parameters of the two proposed filters in comparison with the filter based on the conventional approach are shown in Fig. 21. More expected results are achieved in both examples through the proposed impedance transforming tapped feeds. The slight passband asymmetry and bandwidth shrinkage in both filters are caused for two reasons: 1) the dispersion effects of distributed components and 2) the structure-inherent transmission zero (TZ) contributed by the open-ended stub related to the tapped feed occurring at frequencies on the upper band that can be observed in the following measured results.

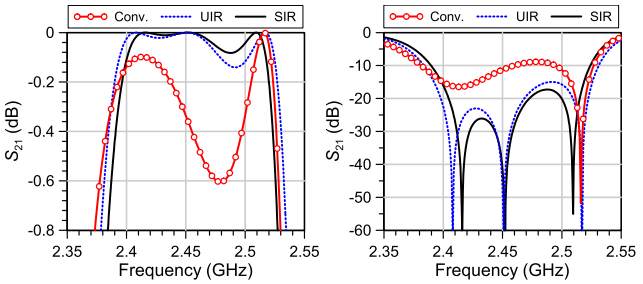

FIGURE 21. Narrowband circuit-level simulated scattering parameters of the two proposed filters (BPF1-UIR and BPF2-SIR) based on the proposed impedance-transforming tapped feeds in comparison with the results of the filter based on the conventional approach (the three filters are all designed for a 3rd-order 0.04321 dB-ripple Chebyshev response with $\Delta = 5\%$).

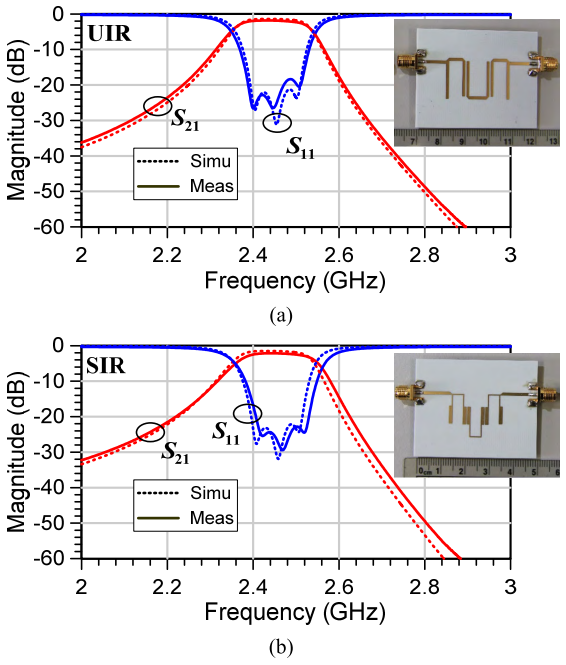

FIGURE 22. Measured and simulated filter-scattering parameters using the accurate impedance transforming tapped feeds. (a) BPF1-UIR. (b) BPF2-SIR.

The two modified filters are then both implemented on a RO4003C substrate ($\varepsilon_r = 3.55$, $h = 0.813$ mm, $\tan\delta = 0.0027$). The narrowband measured and simulated results of the two BPFs are presented in Fig. 22. For the BPF1-UIR, the measured results are a center frequency of 2.45 GHz, the minimum passband IL of 1.82 dB, the worst RL in the passband of 18.37 dB, the 18.37-dB-RL bandwidth of approximately 5.26%, and the 3 dB-IL bandwidth of 7.74%. For the BPF2-SIR, the measured results are a center frequency of 2.46 GHz, the minimum passband IL of 2.14 dB, the worst RL in the passband of 22.25 dB, the 20-dB-RL bandwidth of approximately 5.03%, and the 3 dB-IL bandwidth of 7.95%. Note that the measured ILs of the two proposed BPFs are comparable with those coupled-resonator filters with similar bandwidth published in the literature.

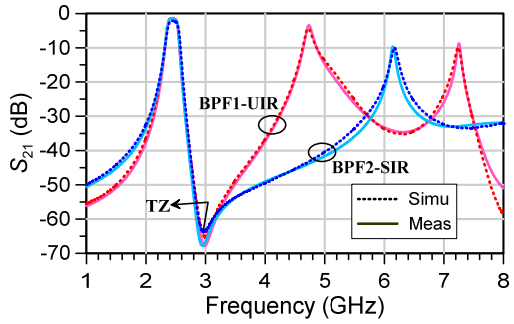

FIGURE 23. Wideband measured and simulated S_{21} of the filters using the accurate impedance-transforming tapped feeds (Red line: BPF1; Blue line: BPF2).

The wideband measured and simulated S_{21} for both filters are shown in Fig. 23. The transmission zero occurring approximately at 3 GHz in both cases contributed by the open-ended stub of the tapped feeds causes passband asymmetry, thus explaining the asymmetric RL ripple observed in the circuit-level simulated results (see Fig. 21). The measured results coincide well with the EM-simulated results for both filters, thus validating the feasibility of the proposed impedance-transforming tapped feeds.

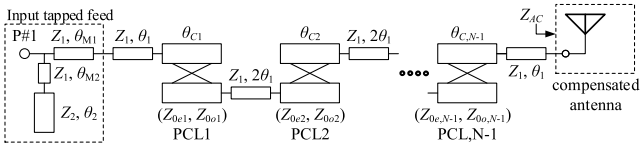

FIGURE 24. *N*th-order filtenna based on the BPF in Fig. 15 ($\theta_U = \theta_2, Z_U = Z_1$).

IV. SYNTHESIS OF THE FILTENNA WITH TAPPED-LINE FEEDS

The filter synthesis approach mentioned in Sec. III can be extended to the filtenna design by treating the antenna as a partial resonator with a radiation resistor constituting the end resonator. An Nth-order filtenna composed of $(N-1)$ PCL sections based on the filter presented in Fig. 15 is depicted in Fig. 24 with $\theta_U = \theta_2$ and $Z_U = Z_1$ to simplify the design. For convenience, let us treat the antenna in the transmitting operation and thus the radiation resistor acts as the output load. Shown in Fig. 25 is a sample antenna model with an additional compensation inductor L_d for demonstration. By utilizing the compensated antenna ($Z_{AC} = R_{AC} + jX_{AC}$) instead of the series resonant load ($Z_{TO} = R_{TO} + jX_{TO}$), the design can be carried out by combining the approaches developed in Secs. II and III. Due to the effect of the compensation inductor, we have Z_{AC} equal to $Z_{ant} = R_{ant} + jX_{ant}$ at the center frequency f_0. The output series resonant load along with the partial $\lambda/4$ resonator constitute the end composite antenna resonator with

$$X_{ant}(f_0) = 0, \frac{x_{NR}(L_{ant}, C_{ant})}{R_{ant}} = Q_{EO}, \tag{27}$$

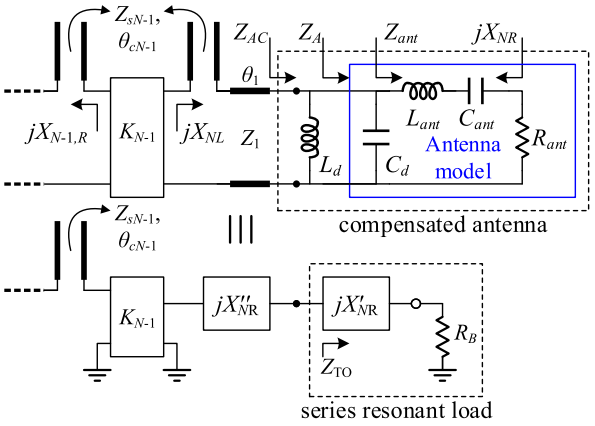

FIGURE 25. Equivalent circuit for determining the output external quality factor related to the end composite antenna resonator.

where $x_{NR} = x'_{NR} + x"_{NR}$ is expressed as

$$x_{NR} = \omega_0 L_{ant} + Z_1 \frac{\sec^2\theta_1[A_Z\theta_2\sec^2\theta_2 + \theta_1(A_Z^2 + \tan^2\theta_2)]}{2(A_Z\tan\theta_1 + \tan\theta_2)^2}. \tag{28}$$

The derived formulas facilitate the determination of the implemented filtenna realizable bandwidth when using different types of antennas. For demonstration, assume all the transmission lines in the equivalent circuit (Fig. 24) are of 50 Ω characteristic impedance and that the filtenna possesses a 3rd-order 0.1-dB-ripple Chebyshev response. The reactance slope parameter of the partial $\lambda/4$ resonator x''_{NR} is 39.27 Ω. The design graph for determining the bandwidth with known (R_{ant}, L_{ant}) and predetermined filter response is drawn in Fig. 27. After finding the element values of the antenna model with respect to the physical dimensions using the EM simulator, the corresponding curve of L_{ant} vs. R_{ant} can then be added to the same figure for finding the related FBW.

V. TWO FILTENNA DESIGN EXAMPLES

Two filtenna types are designed and implemented in this section according to the synthesis procedure described in Sec. IV. Both filtennas are implemented on the 0.508-mm-thick RO4003c substrate ($\varepsilon_r = 3.55$, $\tan\delta = 0.0027$). Note that to provide sufficiently large coupling between resonators, the UIRs are adopted hereafter for longer coupling edges.

A. FILTENNA USING INVERTED-L ANTENNA AND HAIRPIN UIRS

Fig. 26 depicts the filtenna using an inverted-L antenna (ILA) with flattened load resistance and hairpin UIRs. The ILA can be primarily formed from the hairpin filter shown in Fig. 11(a) by removing the port-2 feed line and etching the partial ground under resonator 3. The equivalent circuit of the ILA is identical to the antenna model shown in IV. The equivalent circuit of the utilized compensated ILA is displayed in Fig. 28(a), whereas its simulated input impedances

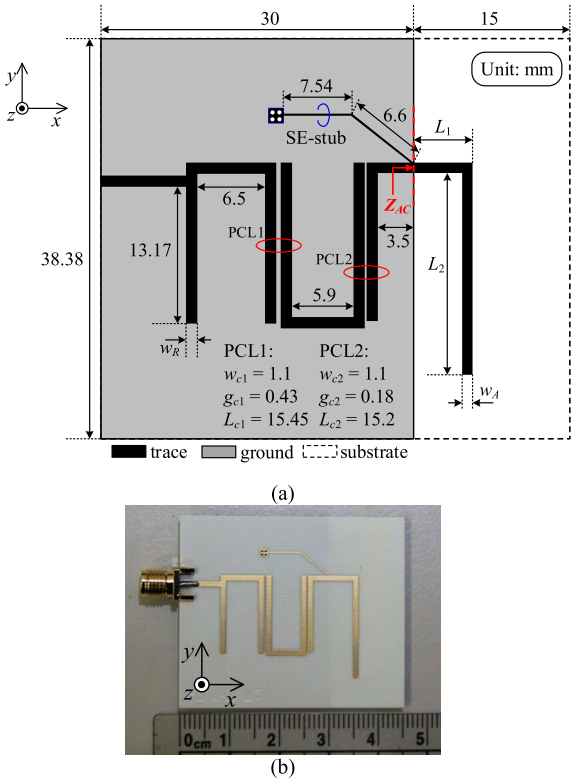

FIGURE 26. (a) Layout and (b) photograph of the proposed filtenna using the compensated ILA with flattened load resistance (Z_{AC} denotes the input impedance of the compensated ILA).

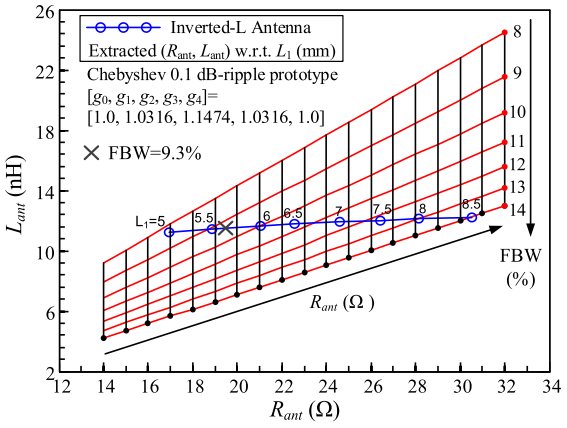

FIGURE 27. Design graph with FBW as a parameter for determining the realizable filtenna FBW after obtaining the extracted antenna resonant parameters R_{ant} and L_{ant} of the ILA (using hairpin UIR with $Z_1 = Z_2 = 50\ \Omega$).

Z_{AC} and the uncompensated counterpart Z_A are compared in Fig. 28(b). The short-ended stub ($Z_{st} = 110\ \Omega$, $\theta_{st} = 55.56°$) is adopted to compensate the shunt capacitor inherently embedded in the original ILA model for flattening the antenna resistance vs. frequency, and the effect is apparently observable from Fig. 28(b). The extracted (R_{ant}, L_{ant}) with respect to the antenna dimension L_1 are included in the design graph (Fig. 27). Based on the design graph, one may pick

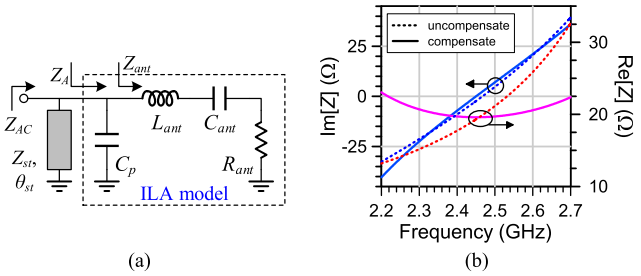

FIGURE 28. Compensated ILA. (a) Equivalent-circuit model. (b) Input impedances of the uncompensated and compensated ILAs (Z_A and Z_{AC}) vs. frequency.

up the required antenna dimensions as the FBW is determined or vice versa.

For demonstration, a 3rd-order filtenna using an ILA with load flattening is designed for a Chebyshev 0.1 dB-ripple response with $f_0 = 2.45$ GHz and $\Delta = 9.3\%$. The element values of the lowpass prototype are [g_0, g_1, g_2, g_3, and g_4] = [1.0, 1.0316, 1.1474, 1.0316, and 1.0]. The corresponding external Qs are $Q_{EI} = Q_{EO} = 11.09$. The hairpin UIRs with $Z_1 = 50\ \Omega$, $Z_2 = 50\ \Omega$, $\theta_1 = 15°$, and $\theta_2 = 75°$ are selected in this case, and the coupled lengths of the two PCL sections are $\theta_C = 75°$. To achieve the required FBW, L_1 is selected as 5.6 mm giving $C_g = 0.395$ pH, $L_{ant} = 11.51$ nH, $C_{ant} = 0.372$ pF, and $R_{ant} = 19.51\ \Omega$. The ILA is compensated by an additional inductor $L_p = 10.68$ nH implemented by a short-ended stub. For the input impedance-transforming tapped feeds, the calculated lengths are $\theta_{M1} = 19.39°$ and $\theta_{M2} = 68.12°$. The even-/odd-mode impedances of the adopted PCLs are $(Z_{0e1}, Z_{0o1}) = (56.53, 43.47)\ \Omega$ and $(Z_{0e2}, Z_{0o2}) = (61.41, 35.59)\ \Omega$, respectively. The circuit-level simulated results along with those transformed from the coupling matrix are presented in Fig. 29 and show great agreement in terms of passband ripple and return loss.

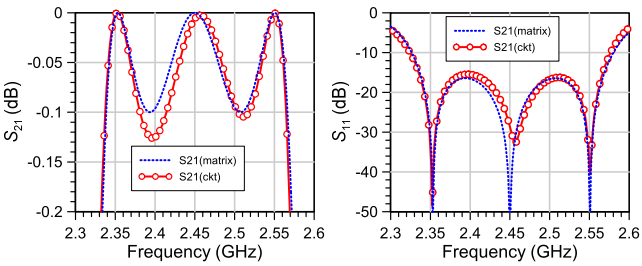

FIGURE 29. Circuit-level two-port scattering parameters of the filtenna in Fig. 24 using the equivalent circuit of the compensated ILA in Fig. 28 by treating R_S and R_{ant} as input and output ports, respectively.

Fig. 30 illustrates the simulated and measured radiation patterns at 2.45 GHz. The pattern of co-polarization on the *yz*-plane is omni-directional as expected. The EM-simulated/measured reflection coefficients, as well as the antenna realized gain vs. frequency, are presented in Fig. 31(a). The minimum RL among the passband is 17.6 dB, whereas the 15-dB RL bandwidth is from 2.342 to

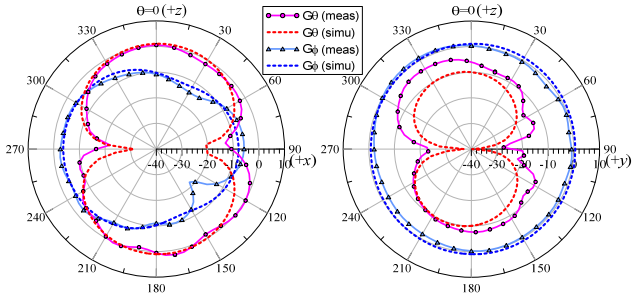

FIGURE 30. EM-simulated and measured radiation patterns of the filtenna using a compensated ILA on the *xz*- and *yz*-planes.

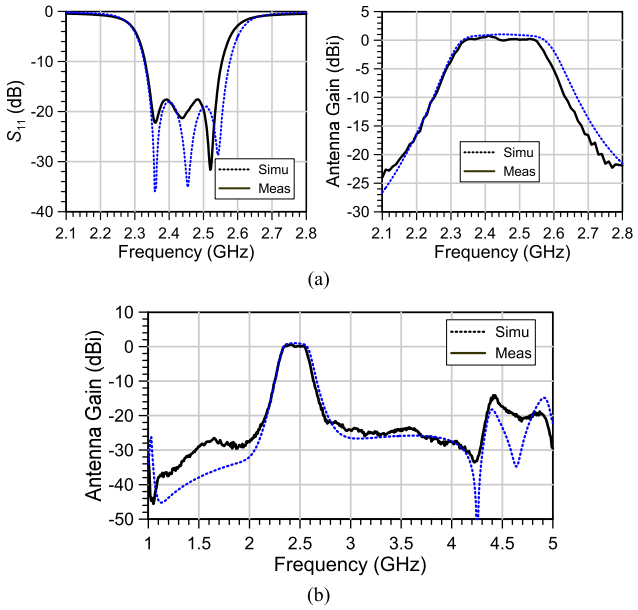

FIGURE 31. EM-simulated and measured results of the proposed ILA filtenna. (a) S_{11} and antenna realized gain in the $+z$ direction ($\varphi = 0°$, $\theta = 0°$) versus frequency. (b) Wideband antenna realized gain.

2.542 GHz related to a ripple-FBW of 8.2%. The simulated and measured antenna gains in the $+z$ direction are approximately 1.022 and 0.79 dBi, respectively, whereas the gain drops below -20 dBi at frequencies below 2.16 GHz or above 2.73 GHz. It is observed that the antenna gain has satisfactory frequency selectivity due to the integrated filter. Fig. 31(b) shows the wideband gain vs. frequency.

B. FILTENNA USING MICROSTRIP-FED SLA AND HAIRPIN UIRS

Recently, the slotline antenna (SLA) [31] has become popular on mobile devices due to the limited design area left for antennas and the trend of using metal cases. Fig. 32 exhibits the layout and photograph of the filtenna using a microstrip-fed SLA with the equivalent model shown in the inset. The 3rd-order filtenna is designed for a Chebyshev 0.04321 dB-ripple response with $\Delta = 9.4\%$. The hairpin UIRs with $Z_1 = 50\ \Omega, Z_2 = 50, \theta_1 = 15°$, and $\theta_2 = 75°$ are selected and the coupled lengths of two PCL sections are 75°. To achieve

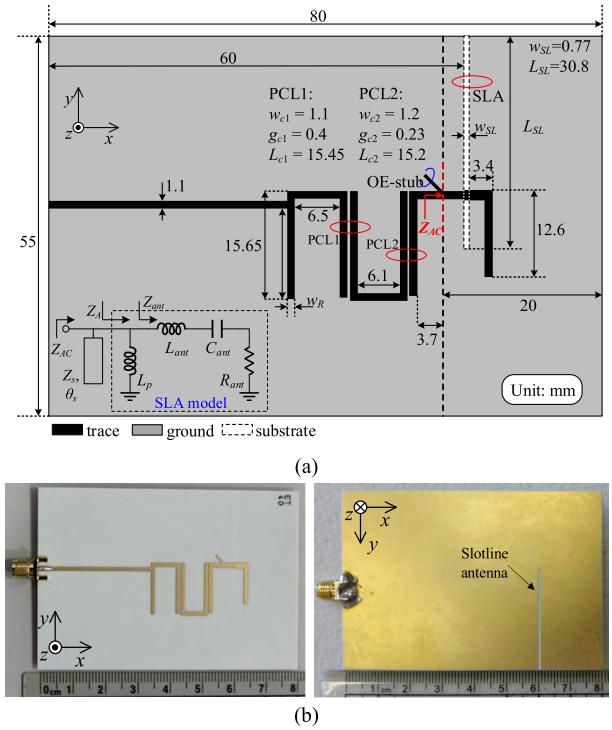

FIGURE 32. (a) Layout and (b) top- and bottom-plane photographs of the proposed filtenna using a microstrip-fed slot antenna with flattened load resistance.

the required FBW, the slotline antenna is designed as shown in Fig. 32 giving ($L_p = 15.17$ pH, $L_{ant} = 6.63$ nH, $C_{\text{ant}} = 0.64$ pF, $R_{\text{ant}} = 15.49\ \Omega$) and compensated by an additional capacitor $C_p = 0.278$ pF implemented by an open-ended stub. The calculated lengths of the input tapped feeds are $\theta_{M1} = 21.02°$ and $\theta_{M2} = 65.73°$. The even-/odd-mode impedances of the adopted PCLs are $(Z_{0e1}, Z_{0o1}) = (57.34, 42.66)\ \Omega$ and $(Z_{0e2}, Z_{0o2}) = (60.45, 39.55)\ \Omega$, respectively.

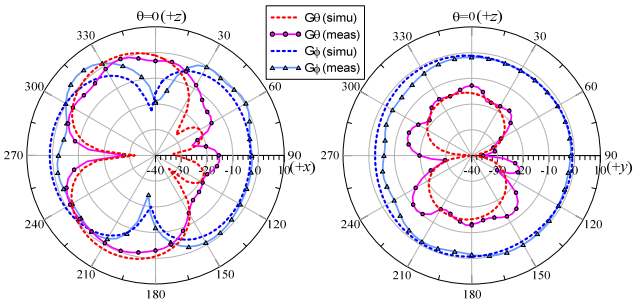

FIGURE 33. EM-simulated and measured radiation patterns of the filtenna using the compensated SLA on the *xz*- and *yz*-planes.

The substrate size is 55×80 mm^2. Fig. 33 illustrates the simulated and measured radiation gain patterns. The EM-simulated and measured reflection coefficients and antenna realized gain in the $+z$ direction ($\varphi = 0°$, $\theta = 0°$) vs. frequency are presented in Fig. 34(a). The minimum RL among the passband is 18.5 dB, whereas the 15-dB

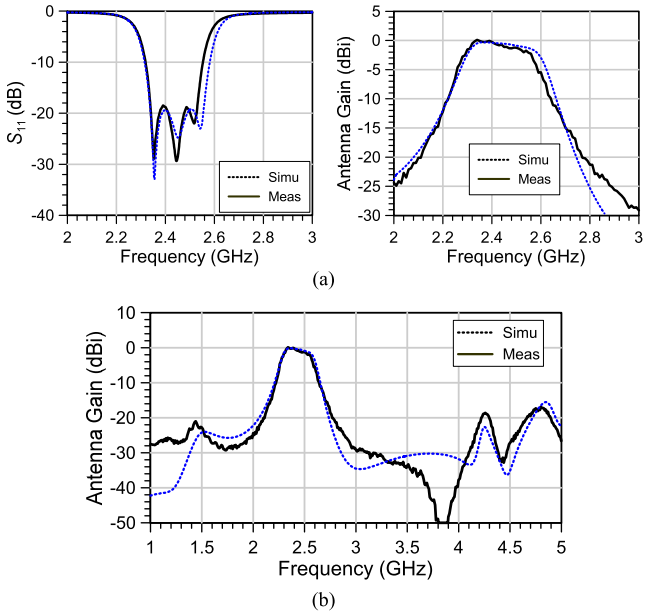

FIGURE 34. EM-simulated and measured results of the proposed SLA filtenna. (a) S_{11} and antenna gains in the $+z$ direction ($\varphi = 0°$, $\theta = 0°$) versus frequency. (b) Wideband antenna realized gains.

RL bandwidth is from 2.333 to 2.539 GHz related to a ripple-FBW of 8.5%. The bandwidth shrinkage may be attributed to the etching resolution of the PCB process. The gain drops lower than −20 dBi at frequencies below 2.12 GHz or above 2.76 GHz, whereas the simulated and measured antenna gains in the $+z$ direction are around -0.301 and 0.118 dBi, respectively. The wideband antenna gains vs. frequency are depicted in Fig. 34(b). The simulations and measurements show satisfactory agreement in terms of frequency response and radiation pattern.

TABLE 4. Comparison between The proposed filtennas and previous works.

	Antenna Type	Resonator Type	Input feed	f_0 (GHz)	FBW (%)
[3]	ILA	Straight UIR	Coupled line	2.45 GHz	14% (Q_A=6~13.7)
[5]	U-shaped patch	T-shaped resonator	Direct feed	5 GHz	2%
[7]	Γ-shaped antenna	Open-loop UIR	Conventional tapped line	2.45 GHz	16.3%
[8]	Rectangular patch	Open-loop UIR	Conventional tapped line	3 GHz	3.4%
Sec. II	PIFA	Straight UIR	Coupled line	2.45 GHz	7.7-13.4%
Sec. V.A	ILA	Hairpin UIR	Accurate impedance transforming tapped feed	2.45 GHz	8-14%
Sec. V.B	SLA	Hairpin UIR		2.45 GHz	8.5%

Table 4 summarizes the performance comparisons between the proposed filtennas and those previous works. The proposed accurate filtenna synthesis approach was utilized in designing three different types of filtennas featuring satisfactory responses in terms of return loss, designable bandwidth, and passband selectivity.

VI. CONCLUSION

In this paper, an accurate filtenna synthesis approach with elaborate design formulas is presented. Compensated antennas are utilized for achieving flattened input resistance, and thus, the filtenna response agrees well with the ideal filter. The load-resistance flattening technique is first verified in a filtenna based on PCL sections using a PIFA. Furthermore, to miniaturize the filtenna size, hairpin resonators and impedance- transforming tapped feeds are incorporated in the design. To validate the proposed modified tapped feeds, two hairpin BPFs with UIRs and with SIRs are designed and implemented. In comparison with conventional tapped-line feeds, the proposed approach ensures the feed structure zero reactance occurs exactly at the filter center frequency guaranteeing the passband performance. By systematically combining the load-resistance flattening technique and the impedance-transforming tapped feeds, an accurate filtenna synthesis procedure is established, and thorough design formulas are derived. Two filtennas using an ILA and an SLA are designed and implemented. To sum up, this study has developed the synthesis procedure applicable for filtennas utilizing several commonly used types of antennas.

ACKNOWLEDGMENTS

The authors would like to thank National Center for High-performance Computing (NCHC) of National Applied Research Laboratories (NARLabs) of Taiwan for providing computational resources and storage resources.

REFERENCES

[1] M. Rotaru, L. Y. Ying, H. Kuruveettil, Y. Rui, A. P. Popov, and C. Chee-Parng, "Implementation of packaged integrated antenna with embedded front end for bluetooth applications," *IEEE Trans. Adv. Packag.*, vol. 31, no. 3, pp. 558–567, Aug. 2008.

[2] J. Zuo, X. Chen, G. Han, L. Li, and W. Zhang, "An integrated approach to RF antenna-filter co-design," *IEEE Antennas Wireless Propag. Lett.*, vol. 8, pp. 141–144, 2009.

[3] C.-T. Chuang and S.-J. Chung, "Synthesis and design of a new printed filtering antenna," *IEEE Trans. Antennas Propag.*, vol. 59, no. 3, pp. 1036–1042, Mar. 2011.

[4] C.-T. Chuang and S.-J. Chung, "A compact printed filtering antenna using a ground-intruded coupled line resonator," *IEEE Trans. Antennas Propag.*, vol. 59, no. 10, pp. 3630–3637, Oct. 2011.

[5] C.-K. Lin and S.-J. Chung, "A compact filtering microstrip antenna with quasi-elliptic broadside antenna gain response," *IEEE Antenna Wireless Propag. Lett.*, vol. 10, pp. 381–384, 2011.

[6] C.-X. Mao, S. Gao, Y. Wang, F. Qin, and Q.-X. Chu, "Multimode resonator-fed dual-polarized antenna array with enhanced bandwidth and selectivity," *IEEE Trans. Antennas Propag.*, vol. 63, no. 12, pp. 5492–5499, Dec. 2015.

[7] W.-J. Wu, Y.-Z. Yin, S.-L. Zuo, Z.-Y. Zhang, and J.-J. Xie, "A new compact filter-antenna for modern wireless communication systems," *IEEE Antennas Wireless Propag. Lett.*, vol. 10, pp. 1131–1134, 2011.

[8] X. Shang and M. J. Lancaster, "Patch antenna with integrated bandpass filter," in *Proc. 4th Annu. Seminar Passive RF Microw. Compon.*, 2013, pp. 1–5.

[9] C. X. Mao, S. Gao, Y. Wang, F. Qin, and Q. X. Chu, "Compact highly integrated planar duplex antenna for wireless communications," *IEEE Trans. Microw. Theory Techn.*, vol. 64, no. 7, pp. 2006–2013, Jul. 2016.

[10] C. X. Mao *et al.*, "Dual-band patch antenna with filtering performance and harmonic suppression," *IEEE Trans. Antennas Propag.*, vol. 64, no. 9, pp. 4074–4077, Sep. 2016.
[11] C.-X. Mao *et al.*, "An integrated filtering antenna array with high selectivity and harmonics suppression," *IEEE Trans. Microw. Theory Techn.*, vol. 64, no. 6, pp. 1798–1805, Jun. 2016.
[12] F.-C. Chen, H.-T. Hu, R.-S. Li, Q.-X. Chu, and M. J. Lancaster, "Design of filtering microstrip antenna array with reduced sidelobe level," *IEEE Trans. Antennas Propag.*, vol. 65, no. 2, pp. 903–908, Feb. 2017.
[13] M.-C. Tang, Y. Chen, and R. W. Ziolkowski, "Experimentally validated, planar, wideband, electrically small, monopole filtennas based on capacitively loaded loop resonators," *IEEE Trans. Antennas Propag.*, vol. 64, no. 8, pp. 3353–3360, Aug. 2016.
[14] J. S. Wong, "Microstrip tapped-line filter design," *IEEE Trans. Microw. Theory Techn.*, vol. MTT-27, no. 1, pp. 44–50, Jan. 1979.
[15] S. B. Cohn, "Parallel-coupled transmission-line-resonator filters," *IRE Trans. Microw. Theory Techn.*, vol. 6, no. 2, pp. 223–231, Apr. 1958.
[16] C.-J. Chen, "Design of parallel-coupled dual-mode resonator bandpass filters," *IEEE Compon., Packag., Manuf. Technol.*, vol. 6, no. 10, pp. 1542–1548, Oct. 2016.
[17] H. Wang, L. Zhu, and W. Menzel, "Ultra-wideband bandpass filter with hybrid microstrip/CPW structure," *IEEE Microw. Wireless Compon. Lett.*, vol. 15, no. 12, pp. 844–846, Dec. 2005.
[18] C. Nguyen, "Broadside-coupled coplanar waveguides and their end-coupled band-pass filter applications," *IEEE Trans. Microw. Theory Techn.*, vol. 40, no. 12, pp. 2181–2189, Dec. 1992.
[19] X. Y. Zhang, X. Dai, H.-L. Kao, B.-H. Wei, Z. Y. Cai, and Q. Xue, "Compact LTCC bandpass filter with wide stopband using discriminating coupling," *IEEE Trans. Compon., Packag., Manuf. Technol.*, vol. CPMT-4, no. 4, pp. 656–663, Apr. 2014.
[20] D. F. Williams and S. E. Schwarz, "Design and performance of coplanar waveguide bandpass filters," *IEEE Trans. Microw. Theory Techn.*, vol. 31, no. 7, pp. 558–566, Jul. 1983.
[21] J. K. A. Everard and K. K. M. Cheng, "High performance direct coupled bandpass filters on coplanar waveguide," *IEEE Trans. Microw. Theory Techn.*, vol. 41, no. 9, pp. 1568–1573, Sep. 1993.
[22] C.-M. Tsai, S.-Y. Lee, and C.-C. Tsai, "Performance of a planar filter using a 0^{circ} feed structure," *IEEE Trans. Microw. Theory Techn.*, vol. 50, no. 10, pp. 2362–2367, Oct. 2002.
[23] J. T. Kuo and E. Shih, "Microstrip stepped impedance resonator bandpass filter with an extended optimal rejection bandwidth," *IEEE Trans. Microw. Theory Techn.*, vol. 51, no. 5, pp. 1554–1559, May 2003.
[24] L.-H. Hsieh and K. Chang, "Tunable microstrip bandpass filters with two transmission zeros," *IEEE Trans. Microw. Theory Techn.*, vol. 51, no. 2, pp. 520–525, Feb. 2003.
[25] K. Ma, J.-G. Ma, K. S. Yeo, and A. V. Do, "A compact size coupling controllable filter with separate electric and magnetic coupling paths," *IEEE Trans. Microw. Theory Techn.*, vol. 54, no. 3, pp. 1113–1119, Mar. 2006.
[26] J.-S. Hong, *Microstrip Filters for RF/Microwave Applications*, 2nd ed. New York, NY, USA: Wiley, 2011.
[27] S. C. Lin, "Coupled-line filters with stub-embedded resonators using accurate admittance-transformer feeds for flexible terminations," *IEEE Trans. Microw. Theory Techn.*, vol. 62, no. 12, pp. 2911–2922, Dec. 2014.
[28] G. L. Matthaei, L. Young, and E. M. T. Jones, *Microwave Filters, Impedance-Matching Networks, and Coupling Structures*. Dedham, MA, USA: Artech House, 1980.
[29] H. R. Ahn and M. M. Tentzeris, "Comments on 'On-chip miniaturized diplexer using joint dual-mode right-/left-handed synthesized coplanar waveguides on GIPD process'," *IEEE Microw. Compon. Lett.*, vol. 26, no. 6, pp. 380–382, Jun. 2016.
[30] E. G. Cristal and S. Frankel, "Hairpin-line and hybrid hairpin-line/half-wave parallel-coupled-line filters," *IEEE Trans. Microw. Theory Techn.*, vol. MTT-20, no. 11, pp. 719–728, Nov. 1972.
[31] K.-L. Wong, P.-W. Lin, and C.-H. Chang, "Simple printed monopole slot antenna for penta-band wireless wide area network operation in the mobile handset," *Microw. Opt. Technol. Lett.*, vol. 53, no. 6, pp. 1399–1404, Jun. 2011.

SHIH-CHENG LIN received the B.S. degree in electrical engineering from National Sun Yat-sen University, Kaohsiung, Taiwan, in 2003, and the Ph.D. degree in communication engineering from National Taiwan University, Taipei, Taiwan, in 2007. In 2007, he joined Taiwan Semiconductor Manufacturing Company, Hsinchu, Taiwan, as an RF-Modeling Engineer. In 2008, he joined Sunplus Technology Company Ltd., Hsinchu, Taiwan, as an Advanced Engineer involving in RF integrated circuit design. Since 2009, he has been with the Department of Electrical Engineering, National Chiayi University, Chiayi, Taiwan, where he is currently a Professor. His research interests include development and design of microwave passive components, RF/microwave integrated circuits, and phased array antennas.

PIN-YAO CHIOU was born in Kaohsiung, Taiwan, in 1992. He received the B.Sc. degree in electrical engineering from the National Hsinchu University of Education, Hsinchu, Taiwan, in 2015, and the M.Sc. degree in electrical engineering from National Chung Cheng University, Taiwan, in 2017. He is currently an RF Engineer with Foxconn Electronics Inc., Taiwan.

YI-MING CHEN received the M.S. degree in computers and communication from Shu-Te University, Taiwan, in 2003, and the Ph.D. degree in electrical engineering at National Chung Cheng University, Taiwan, in 2010. From 2010 to 2018, He was a Post-Doctoral Research Fellow with the Institute Center for Telecommunication Research. He was also an Adjunct Assistant Professor of electrical engineering with the National Chung Cheng University, Taiwan. He is currently an RF Engineer with Foxconn Electronics Inc., Taiwan. His research interests include the design and analysis of passive components for microwave and millimeter-wave applications.

SHENG-FUH CHANG received the B.S. and M.S. degrees in communications engineering from National Chiao-Tung University, Taiwan, in 1982 and 1984, respectively, and the Ph.D. degree in electrical engineering from the University of Wisconsin at Madison in 1991. He was with the Center for Plasma Theory and Computation, University of Wisconsin at Madison, involved in high-power microwave and millimeter-wave sources, including free-electron lasers and Cerenkov masers. In 1992, he joined Hyton Technology Corporation, where he was e for C- and Ku-band satellite low-noise down-converter and multiple-channel multipoint distribution system transceivers. In 1994, he joined the Department of Electrical Engineering, National Chung Cheng University, Taiwan, where he is currently a Full Professor with the Department of Electrical Engineering and the Department of Communications Engineering, and the Director of the Center for Telecommunication Research. His research interests include micro-power electromagnetic vital signal detection, wireless indoor locating techniques, multiantenna beamforming systems, and microwave/millimeter-wave monolithic integrated circuits for broadband wireless RF transceivers.

Dr. Chang is a member of the Phi Tau Phi and Sigma Xi.